COMPUTATIONAL ANALYSIS OF THE AERODYNAMIC HEATING AND DRAG OF A REENTRY BRAZILIAN SATELLITE

Pedro A. C. Sampaio, andrey@lcp.inpe.br
Wilson F. N. Santos, wilson@lcp.inpe.br

Combustion and Propulsion Laboratory, National Institute for Space Research, Cachoeira Paulista, SP 12630-000

Abstract *The aim of the work reported here is to present a computational investigation on the small ballistic reentry Brazilian vehicle SARA (acronym for SAtélite de Reentrada Atmosférica). Chemical equilibrium and thermal non-equilibrium hypersonic flow over the vehicle SARA at zero-degree angle of attack is modeled by the Direct Simulation Monte Carlo (DSMC) method. The emphasis of this paper is to examine the behavior of the aerodynamic surface quantities during the high altitude portion of the SARA reentry. In this fashion, pressure, skin friction, heat transfer and drag coefficients are investigated for altitudes of 100, 95, 90 and 85 km. In addition, comparisons based on geometry are made by considering axisymmetric and planar two-dimensional configurations. The analysis showed that the stagnation region is a thermally stressed zone. The peak value for the heat flux was attained at the stagnation point. It was also found that the stagnation region is a zone of strong compression, high wall pressure.*

Keywords: *DSMC, rarefied flow, hypersonic flow, aerodynamic heating, reentry.*

1. INTRODUCTION

The initiatives in the space area have received a new impulse with the Brazilian Program for Space Activities, officially called PNAE (acronym for Programa Nacional de Atividades Espaciais). The main objective of the PNAE is to encourage the capacity of the country in order to utilize space resources and techniques, and to solve national problems for the benefit of the Brazilian society. Currently, one of the major programs of PNAE is related to a reusable orbital platform, named SARA (acronym for SAtélite de Reentrada Atmosférica), for scientific and technological experiments in low gravity environment. The system, build in a platform with a capsule shape, will stay in orbit during the time needed for the execution of the experiments, being sent back to the Earth, and then recovered.

The development of experiments in a microgravity environment by using a reusable space vehicle (capsule) has lately drawn considerable interest in the aerothermodynamics of this vehicle along the entire flight trajectory. The computation of the aerothermodynamics of hypersonic reentry vehicles along their entire trajectory involves rarefied conditions at high altitudes and continuum conditions at low altitudes. For each of these flow regimes, well established simulation methods already exist. For instance, the particle based Direct Simulation Monte Carlo (DSMC) method may be used for the rarefied flows, and the continuum Navier-Stokes equations may be solved by using algorithms from Computational Fluid Dynamics (CFD).

Aerothermodynamic analysis plays a critical role in designing a vehicle for hypersonic fight. Accurate information on the vehicle aerodynamics along the descent trajectory allow one to understand the capsule performance and, therefore, increase the payload and reduce the heat-shield thickness on the vehicle. One of the main concerns of the aerodynamics of planetary entry is the heating rate and the damage that this may cause to the vehicle at hypersonic flight speed. The maximum heat flux to the structure usually occurs at the stagnation point of the vehicle. This maximum heat flux is inversely proportional to the square root of the nose radius.

Many numerical studies and a few experimental investigations (Carlson, 1999; Gilmore and Crowther, 1995; Gnoffo, 1999; Gupta *et al.*, 1996; Ivanov *et al.*, 1998; Longo, 2003; Moss, 2006; Savino *et al.*, 2005; Vashchenkov and Ivanov, 2002; Weiland *et al.*, 2004; Wilmoth *et al.*, 1997; Wood *et al.*, 1996) have been dedicated to the aerothermodynamics of vehicles reentering the Earth atmosphere. Nevertheless, for the particular case of SARA capsule, only a few studies are available in the current literature (Pimentel *et al.*, 2005; Sharipov, 2003; Tchuen *et al.*, 2005; Toro *et al.*, 2001; Sampaio and Santos, 2009). For the purpose of this introduction, it will be sufficient to describe only a few of these studies.

Sharipov (2003) investigated the flowfield structure over the SARA capsule by employing the DSMC method. Argon was assumed as a working fluid with Mach numbers of 5, 10, and 20. Even considering that the real gas effect in a reentry capsule can not be simulated by a monatomic gas, that investigation might be considered as the first contribution to the

aerothermodynamic analysis of the SARA capsule at high altitudes.

Pimentel *et al.* (2005) performed inviscid hypersonic flow simulations over the SARA capsule modeled by the planar two-dimensional and by the axisymmetric Euler equations. Results were presented for an altitude of 80 km, Mach numbers of 15 and 18, and angle of attack of 0 and 10 degrees. They also considered air as working fluid composed of five species (N_2, O_2, O, N, and NO) and their reactions of dissociation and recombination. Pressure and temperature contours were presented for 2-D and axisymmetric flows.

By using axisymmetric Navier-Stokes equations, Tchuen *et al.* (2005) have investigated the flowfield structure over the SARA capsule by considering hypersonic flow at zero angle of attack in chemical and thermal non-equilibrium. It was assumed air as working fluid composed of seven species (N_2, O_2, O, N, NO, NO^+, and e^-) and their reactions of dissociation and recombination. Results for pressure, skin friction, and heat transfer coefficients were presented for different combinations of Mach numbers of 10, 20 and 25 with altitudes of 75 and 80 km.

Finally, by using the DSMC method, Sampaio and Santos (2009) have investigated the flowfield structure of a hypersonic flow over the SARA capsule in the reentry trajectory from 100 km to 85 km. This range basically covered the transition flow regime, *i.e.*, between the free collision flow and the continuum flow regime. The primary goal was to assess the sensitivity of the primary properties, velocity, density, pressure, and temperature due to changes on the altitude representative of a typically reentry trajectory of the SARA capsule.

The present account extends the analysis presented by Sampaio and Santos (2009) by examining computationally the aerodynamic surface quantities on the SARA capsule for the same reentry conditions. In this fashion, the purpose of the present account is to assess the sensitivity of the heat transfer, pressure, skin friction and drag coefficients in the reentry trajectory from 100 km to 85 km. Therefore, the present study focuses on the low-density region in the upper atmosphere, where the non-equilibrium conditions are such that traditional CFD calculations are inappropriate to yield accurate results. In such a circumstance, the Direct Simulation Monte Carlo (DSMC) method will be employed to calculate the planar two-dimensional and the axisymmetric hypersonic flow over the SARA capsule.

2. GEOMETRY DEFINITION

The SARA reentry capsule is an axisymmetric design consisting of a spherical nose with a 11.4-degree half-angle conical afterbody(Sampaio and Santos, 2009). The nose radius R is 0.2678 m, the afterbody base has a radius R_B of 0.5035 m, and the total length L is 1,410 m. Figure (1) illustrates schematically the capsule shape and the main important physical and geometric parameters related to the hypersonic flow on the capsule. The main physical parameters are defined as follows: M_∞ is the freestream Mach number, Kn_∞ stands for the Knudsen number, α is the angle of attack, T_w is the wall temperature, and finally, α_n and σ_t represent the parameters related to the gas-surface interaction. In this fashion, the flowfield structure around the capsule may be affected by the effects of compressibility, rarefaction, gas-surface interaction, etc.
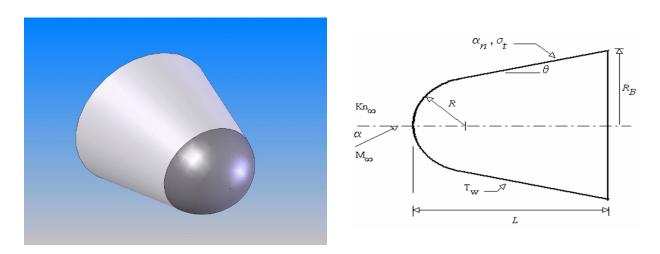

Figure 1. Drawing illustrating (a) a schematic view of the capsule and (b) the important parameters.

3. COMPUTATIONAL METHOD AND PROCEDURE

The most successful numerical technique for modeling complex transitional flows has been the Direct Simulation Monte Carlo (DSMC) method (Bird, 1994). The DSMC method simulates real gas flows with various physical processes by means of a huge number of modeling particles, each particle represents a fixed number of real gas molecules. In the

DSMC model, the particle evolution is divided into two independent phases during the simulation; the movement phase and the collision phase. In the movement phase, all particles are moved over distances appropriate to a short time interval, time step, and some of them interact with the domain boundaries in this time interval. Particles that strike the solid wall would reflect according to the appropriate gas-surface interaction model, specular, diffusive or a combination of these. In the collision phase, intermolecular collisions are performed according to the theory of probability without time being consumed. In this scenario, the intermolecular collisions are uncoupled to the translational molecular motion over the time step used to advance the simulation. Time is advanced in discrete steps such that each step is small in comparison with the mean collision time. The simulation is always calculated as unsteady flow. However, a steady flow solution is obtained as the large time state of the simulation.

In the present account, collisions are modeled by using the variable hard sphere (VHS) molecular model (Bird, 1981) and the no time counter (NTC) collision sampling technique (Bird, 1989). The VHS model employs the simple hard sphere angular scattering law so that all directions are equally possible for post-collision velocity in the center-of-mass frame of reference. Nevertheless, the collision cross section depends on the relative speed of colliding molecules according to some power law. The exponent is calculated by matching the viscosity of the simulated gas to that of its real counterpart. The mechanics of the energy exchange processes between kinetic and internal modes for rotation and vibration are controlled by the Borgnakke-Larsen statistical model (Borgnakke and Larsen, 1975). The essential feature of this model is that part of collisions is treated as completely inelastic, and the remainder of the molecular collisions is regarded as elastic. For a given collision, the probabilities are designated by the inverse of the relaxation numbers, which correspond to the number of collisions necessary, on average, for a molecule to relax. In this study, the relaxation numbers of 5 and 50 were used for the rotation and vibration, respectively. Simulations are performed using a non-reacting gas model consisting of two chemical species, N_2 and O_2.

4. COMPUTATIONAL FLOW DOMAIN AND GRID

For the numerical treatment of the problem, the flowfield around the capsule is divided into an arbitrary number of regions, which are subdivided into computational cells. The cells are further subdivided into subcells, two subcells/cell in each coordinate direction. The cell provides a convenient reference for the sampling of the macroscopic gas properties, while the collision partners are selected from the same subcell for the establishment of the collision rate. Therefore, the physical space network is used to facilitate the choice of molecules for collisions and for the sampling of the macroscopic flow properties such as temperature, pressure, density, etc.

The computational domain used for the calculation is made large enough so that body disturbances do not reach the upstream and side boundaries, where freestream conditions are specified. In this manner, the computational domain changed according to the rarefaction degree of the flow hitting the capsule. A schematic view of the computational domain is depicted in Fig. (2a). Side I is defined by the body surface. Diffuse reflection with complete thermal accommodation is the condition applied to this side. In a diffuse reflection, the molecules are reflected equally in all directions, and the final velocity of the molecules is randomly assigned according to a half-range Maxwellian distribution determined by the wall temperature. Advantage of the flow symmetry is taken into account, and molecular simulation is applied to one-half of a full configuration. Thus, side II is a plane of symmetry, where all flow gradients normal to the plane are zero. At the
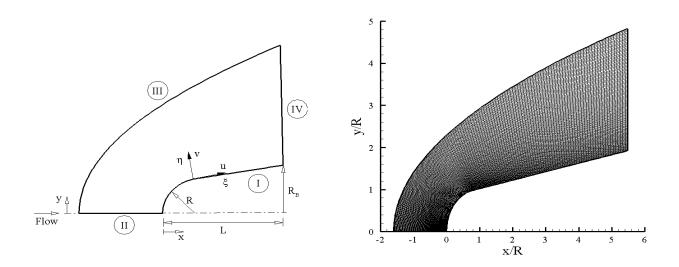

Figure 2. Drawing illustrating (a) the computational domain and (b) the standard grid for the 90 km case.

molecular level, this plane is equivalent to a specular reflecting boundary. Side III is the freestream side through which simulated molecules enter and exit. Finally, the flow at the downstream outflow boundary, side IV, is predominantly supersonic and vacuum condition is specified (Bird, 1994). At this boundary, simulated molecules can only exit.

The numerical accuracy in DSMC method depends on the cell size chosen, on the time step as well as on the number of particles per computational cell. In the DSMC algorithm, the linear dimensions of the cells should be small in comparison with the length scale of the macroscopic flow gradients normal to streamwise directions, which means that the cell dimensions should be the order of or smaller than the local mean free path (Alexander $et\ al.$, 1998, 2000). The time step should be chosen to be sufficiently small in comparison with the local mean collision time (Garcia and Wagner, 2000; Hadjiconstantinou, 2000). In general, the total simulation time, discretized into time steps, is based on the physical time of the real flow. Finally, the number of simulated particles has to be large enough to make statistical correlations between particles insignificant.

These effects were investigated in order to determine the number of cells and the number of particles required to achieve grid independent solutions. A grid independence study was made with three different structured meshes in each coordinate direction. The effect of altering the cell size in the ξ-direction was investigated with grids of 60 (coarse), 120 (standard) and 180 (fine) cells, and 110 cells in the η-direction for the 90 km case. In analogous fashion, an examination was made in the η-direction with grids of 55 (coarse), 110 (standard) and 165 (fine) cells, and 120 cells in the ξ-direction for the same case. From the total number of cells in the ξ-direction, 50 cells are located along the spherical nose and 70 cells distributed along the afterbody surface. In addition, each grid was made up of non-uniform cell spacing in both directions. The effect (not shown) of changing the cell size in both directions on the heat transfer, pressure and the skin friction coefficients was rather insensitive to the range of cell spacing considered, indicating that the standard grid, 120 X 110 cells, for the 90 km case, is essentially a grid independent. Figure (2b) illustrates the standard grid for the 90 km case.

A similar examination was made for the number of molecules. The standard grid for the 90 km case, 120 X 110 cells, corresponds to, on average, a total of 277,000 molecules. Two new cases using the same grid were investigated. These two new cases correspond to 131,600 and 396,100 molecules in the entire computational domain. As the three cases presented approximately the same results (not shown) for the heat transfer, pressure and skin friction coefficients, hence the standard grid with a total of 277,000 molecules is considered enough for the computation of the aerodynamic surface quantities.

5. FREESTREAM AND FLOW CONDITIONS

Flow conditions represent those experienced by the SARA capsule in the reentry from 100 to 85 km of altitude. The freestream flow conditions used for the numerical simulation of flow past the capsule are those given by Sampaio and Santos (2009) and summarized in Tab. (1), and the gas properties (Bird, 1994) are shown in Tab. (2). Referring to Tab. (1), T_∞, p_∞, ρ_∞, n_∞, λ_∞, and V_∞ stand respectively for temperature, pressure, density, number density, molecular mean free path, and velocity. According to Tab. (2), X, m, d and ω account respectively for mass fraction, molecular mass, molecular diameter and viscosity index.

Table 1. Freestream flow conditions

Altitude (km)	T_∞(K)	p_∞(N/m^2)	ρ_∞(kg/m^3)	n_∞(m^{-3})	λ_∞(m)	V_∞(m/s)
85	180.7	0.41249	7.956×10^{-6}	1.6539×10^{20}	7.751×10^{-3}	7864
90	180.7	0.16438	3.171×10^{-6}	6.5908×10^{19}	1.945×10^{-2}	7864
95	195.5	0.06801	1.212×10^{-6}	2.5197×10^{19}	5.088×10^{-2}	7866
100	210.0	0.03007	4.989×10^{-7}	1.0372×10^{19}	1.236×10^{-1}	7862

According to the velocity-altitude map for the SARA capsule (Pessoa Filho, 2008), for altitudes of 85, 90, 95 and 100 km, the freestream velocity V_∞ is 7864, 7864, 7866, and 7862 m/s, respectively. These values correspond to a freestream Mach number M_∞ of 29.2, 29.2, 28.1, and 27.1, respectively. In the present account, the capsule surface was kept at a constant wall temperature T_w of 800 K for all cases investigated. This temperature is chosen to be representative of the surface temperature near the stagnation point of a reentry capsule. According to Machado and Boas (2006), in the stagnation region of the SARA capsule, temperature may reach a value around 950 K.

Table 2. Gas properties

	X	m (kg)	d (m)	ω
O_2	0.237	5.312×10^{-26}	4.01×10^{-10}	0.77
N_2	0.763	4.650×10^{-26}	4.11×10^{-10}	0.74

The overall Knudsen number Kn is defined as the ratio of the molecular mean free path λ in the freestream gas to a

characteristic dimension of the flowfield. In the present study, the characteristic dimension was defined as being the nose radius R. For the altitudes investigated, 85, 90, 95, and 100 km, the overall Knudsen numbers correspond to Kn_R of 0.0289, 0.0726, 0.1899 and 0.4615, respectively. The Reynolds number Re_R correspond to 15249.5, 609.1, 224.1, and 92.2 for altitudes of 85, 90, 95, and 100 km, respectively, based on conditions in the undisturbed stream with the nose radius R as the characteristic length. Finally, zero-degree angle of attack was considered in this investigation.

6. COMPUTATIONAL RESULTS AND DISCUSSION

The rarefied effects on the aerodynamic surface quantities acting on the SARA capsule are demonstrated in this section by comparing the simulated results for freestream Knudsen numbers of 0.4615, 0.1899, 0.0726, and 0.0289, which correspond to altitudes of 100, 95, 90 and 85 Km, respectively. Aerodynamic surface quantities of particular interest in the transition flow regime are number flux, heat flux, wall pressure, shear stress, and drag. In order to assess the dependence of the aerodynamic forces and heat transfer on the altitude or freestream Knudsen number, simulations were conducted based on those parameters related to the SARA reentry trajectory, as defined by Tab. (1).

6.1 Number Flux

The number flux N is calculated by sampling the molecules impinging on the surface by unit time and unit area. The distribution of the number flux along the capsule surface is illustrated in Figs. (3a-c) for altitudes of 100, 90 and 85 km, respectively, by considering 2-D planar and axisymmetric configurations. In this group of plots, N_f represents the number flux N normalized by $n_\infty V_\infty$, where n_∞ is the freestream number density and V_∞ is the freestream velocity. In addition, s/R is the arc length s normalized by the nose radius R. It is important to mention that results for the 95 km case are intermediate to those for 100 km and 90 km and, therefore, they will no be shown.

According to this set of plots, it is seen that the number flux to the surface presents essentially a similar behavior for both configurations, i.e., 2-D planar and axisymmetric one. In general, the curves show two distinct regions: one inner region, along the spherical nose (cylindrical nose for the 2-D case), and a outer region, along the cone surface (wedge surface for the 2-D case). In the inner region, at the vicinity of the stagnation point, the number flux is basically constant. In this inner region the number flux presents its maximum value. In addition, in this region, the number flux increases with decreasing the altitude. An expected behavior since the number density n_∞ increases with a reduction in the altitude. Afterwards, the number flux drastically decreases and reaches basically a constant value along the wedge surface, for the 2-D case, or the cone surface for the axisymmetric configuration.

In order to emphasize points of interest, the number flux distribution along the spherical nose (axisymmetric case) or the cylindrical nose (2-D case) is displayed in Figs. (4a-c) for altitudes of 100, 90 and 85 km, respectively, as a function of the slope angle θ, measured from the stagnation point at the nose. For comparison purpose, these plots display the number flux by assuming free molecular flow (FM) or collisionless flow. According to this set of plots, it is clearly seen that as the altitude increases the number flux N_f decreases at the vicinity of the stagnation region and tends to the free molecular limit obtained by the free molecular flow equations.
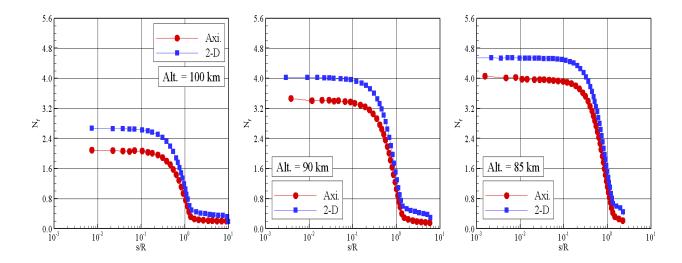

Figure 3. Distribution of the dimensionless number flux N_f along the capsule surface for altitudes of (a) 100 km, (b) 90 km, and (c) 85 km.
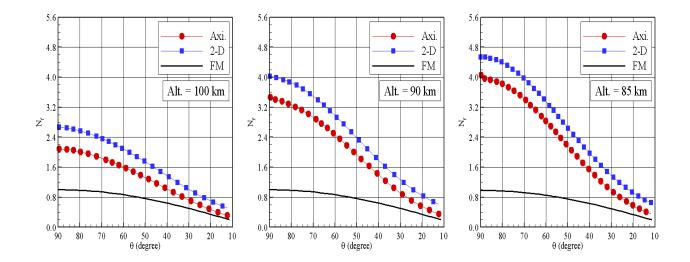
Figure 4. Distribution of the dimensionless number flux N_f along the capsule surface as a function of the body slope angle θ for altitudes of (a) 100 km, (b) 90 km, and (c) 85 km.

6.2 Heat Transfer Coefficient

The heat transfer coefficient C_h is defined as follows,

$$C_h = \frac{q_w}{\frac{1}{2}\rho_\infty V_\infty^3} \tag{1}$$

where the heat flux q_w to the body surface is calculated by the net energy flux of the molecules impinging on the surface. A flux is regarded as positive if it is directed toward the body surface. The net heat flux q_w is related to the sum of the translational, rotational and vibrational energies of both incident and reflected molecules as defined by,

$$q_w = q_i - q_r = \sum_{j=1}^{N}[\frac{1}{2}m_j c_j^2 + e_{Rj} + e_{Vj}]_i - \sum_{j=1}^{N}[\frac{1}{2}m_j c_j^2 + e_{Rj} + e_{Vj}]_r \tag{2}$$

where N is the number of molecules colliding with the surface by unit time and unit area, m is the mass of the molecules, c is the velocity of the molecules, e_R and e_V stand for the rotational and vibrational energies, respectively. Subscripts i and r refer to incident and reflect molecules.

The dependence of the heat transfer coefficient C_h on the altitude is demonstrated in Figs. (5) and (6). Figures (5a-c) demonstrate the heat transfer coefficient C_h along the capsule surface as a function of the arc length s/R, while Figs. (6a-c) display C_h as a function of the body slope angle θ. The heat transfer coefficient C_h predicted by assuming free molecular flow is also included for reference in Figs. (6a-c).

Based on this set of diagrams, it is clearly noticed that the heat transfer coefficient C_h is sensitive not only to the body shape but also to the altitude, $i.e.$, to the Knudsen number Kn_R. The heat transfer coefficient C_h presents the maximum value at the stagnation point. After that, a short distance away of the stagnation point, it drops off up to the sphere/cone junction (for axisymmetric case) or to the cylinder/wedge junction (for 2-D case). It is also seen that as the altitude increases, $i.e.$, the Knudsen number increases, the heat transfer coefficient C_h increases and approaches the free molecular value for the conditions investigated in this work. As the altitude increases, the freestream density decreases, and the denominator in Eq. (1) decreases. Consequently, an increase in the heat transfer coefficient C_h is observed.

According to Figs. (5) and (6), the heat flux to the capsule surface is most severe at the stagnation point. Theoretical and numerical predictions of stagnation point heat transfer for continuum flow have been developed by Fay and Riddell (1958); Lees (1956); Sibulkin (1952); Roming (1958), to name a few. The work of Fay and Riddell (1958) is the typical reference point on aerodynamic heating. Due to their simplicity, the Fay-Riddell correlation formulas are still in use today for the thermal analysis of hypersonic vehicles, although the formulas suffer from inaccuracies that reduces the validity of the results, as pointed by Zuppardi and Verde (1998). Theoretical formulations, experimental data, and semi-empirical formulas all agree in the fact that stagnation point heat transfer is inversely proportional to the square root of the nose radius.
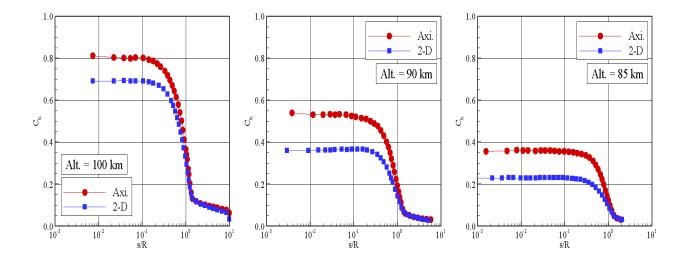
Figure 5. Distribution of heat transfer coefficient C_h along the capsule surface for altitudes of (a) 100 km, (b) 90 km, and (c) 85 km.
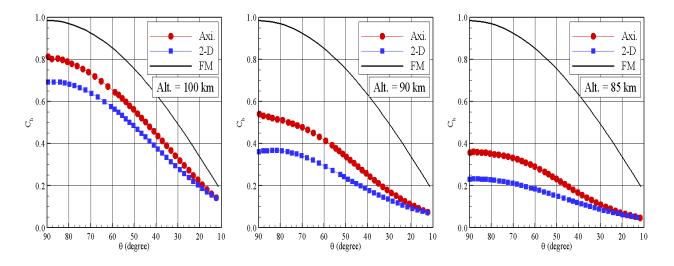

Figure 6. Distribution of heat transfer coefficient C_h along the capsule surface as a function of the body slope angle θ for altitudes of (a) 100 km, (b) 90 km, and (c) 85 km.

6.3 Pressure Coefficient

The pressure coefficient C_p is defined as follows,

$$C_p = \frac{p_w - p_\infty}{\frac{1}{2}\rho_\infty V_\infty^2} = \frac{p_w/p_\infty - 1}{\frac{1}{2}\gamma_\infty M_\infty^2} \qquad (3)$$

where γ_∞ is the freestream specific heat ratio, and the pressure p_w on the body surface is calculated by the sum of the normal momentum fluxes of both incident and reflected molecules at each time step as follows,

$$p_w = p_i - p_r = \sum_{j=1}^{N}\{[(mv)_j]_i - [(mv)_j]_r\} \qquad (4)$$

where v is the velocity component of the molecule j in the surface normal direction.

The impact of rarefaction on the pressure coefficient C_p along the capsule surface as a function of the arc length s/R is depicted in Figs. (7a-c) for 100, 90 and 85 km of altitude, respectively. In addition, Figs. (8a-c) illustrate the pressure
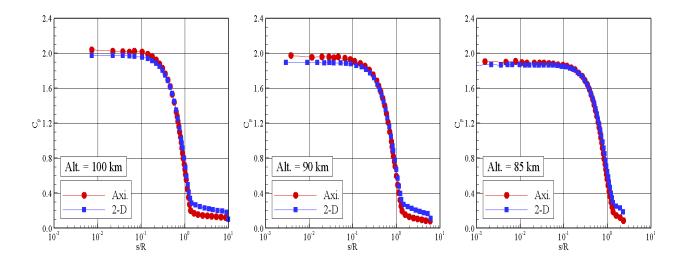
Figure 7. Distribution of pressure coefficient C_p along the capsule surface for altitudes of (a) 100 km, (b) 90 km, and (c) 85 km.
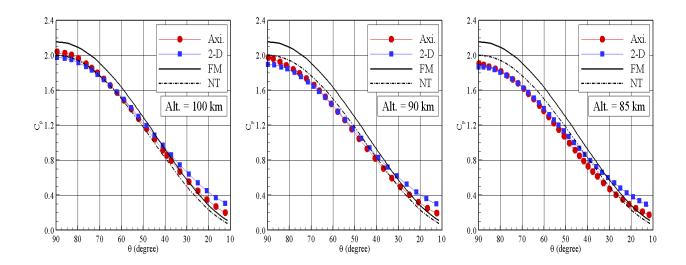

Figure 8. Distribution of pressure coefficient C_p along the capsule surface as a function of the body slope angle θ for altitudes of (a) 100 km, (b) 90 km, and (c) 85 km.

coefficient C_p as a function of the body slope angle θ. Plotted along with the computational solutions for pressure coefficient is the pressure coefficient C_p predicted by the Newtonian theory (NT), $C_p = 2sin^2\theta$, and by considering free molecular flow (FM). As plotted in this way, the pressure coefficients predicted by both Newtonian theory and free molecular flow are independent of the body shape, and they represent any geometry where the body slope angle changes from 90 degree at the nose to 11.4 degree downstream of the nose.

Looking first at Figs. (7a-c), it is observed that the pressure coefficient C_p acting on the SARA capsule surface follows the same trend as that presented by the number flux, Fig. (4), in the sense that C_p is maximum in the stagnation region. After that, C_p drastically decreases up to the sphere/cone junction (for axisymmetric case) or to the cylinder/wedge junction (for 2-D case). Along the cone or wedge surface, the pressure coefficient C_p is basically constant, with values one order of magnitude lower than those attained in the stagnation point.

Turning next to Figs. (8a-c), it may be recognized that, for high Knudsen numbers, i.e., high altitudes, the pressure coefficient C_p basically follows the same behavior of that obtained by the Newtonian theory. According to the Newtonian concept, the air flowing around a body is undisturbed by the presence of the body until it strikes the solid surface, at which time the air loses the component of momentum normal do the surface. The Newtonian theory takes into account only for the directed movement of the molecules not to the random movement of the molecules. In a hypersonic flow, the directed movement of the molecules is much larger than the random movement. Finally, it should be emphasized that, although

the pressure coefficient C_p is basically the same for the altitudes investigated, the pressure acting on the capsule surface, p_w, is different for each altitude. This is quite apparent from Eq. (3), since the freestream pressure, p_∞ and the freestream dynamic pressure, $\frac{1}{2}\rho_\infty V_\infty^2$, are different for each altitude.

6.4 Skin Friction Coefficient

The skin friction coefficient C_f is defined as follows,

$$C_f = \frac{\tau_w}{\frac{1}{2}\rho_\infty V_\infty^2} = \frac{\tau_w/p_\infty}{\frac{1}{2}\gamma_\infty M_\infty^2} \tag{5}$$

where the shear stress τ_w on the body surface is calculated by the sum of the tangential momentum fluxes of both incident and reflected molecules impinging on the surface at each time step by the following expression,

$$\tau_w = \tau_i - \tau_r = \sum_{j=1}^{N}\{[(mu)_j]_i - [(mu)_j]_r\} \tag{6}$$

where u is the velocity component of the molecule j in the surface tangential direction.

It is worthwhile to note that for the special case of diffuse reflection, the gas-surface interaction model adopted herein, the reflected molecules have a tangential moment equal to zero, since the molecules essentially lose, on average, their tangential velocity components. In this fashion, the reflected tangential momentum flux is zero, *i.e.*, $\tau_r = 0$.

The rarefaction effect on the skin friction coefficient C_f along the SARA capsule surface is demonstrated in Figs. (9a-c) for altitudes of 100, 90 and 85 km, respectively. Along the capsule surface, C_f starts from zero at the stagnation point, increases to a maximum value located on the spherical surface (for axisymmetric case) or cylindrical surface (for 2-D case), and decreases downstream along this surface up to the junction point. Larger altitude leads to higher peak value for the skin friction coefficient C_f.

The skin friction coefficient C_f presents interesting features as it is plotted as a function of the body slope angle θ. Figures (10a-c) show these features as well as a comparison with the skin friction coefficient by assuming a free molecular flow. As can be seen, the skin friction coefficient C_f predicted by free molecular flow exhibits its maximum value at a station corresponding to 45 degrees. For the sphere/cone shape, the maximum value for the skin friction coefficient C_f takes place at station corresponding to 48.6, 51.4, and 52.7 degrees for altitude of 100, 90 and 85 km, respectively. As a result, as the altitude increases, *i.e.*, the Knudsen number Kn_R increases, the pick value approaches the limit value predicted by the free molecular flow.

6.5 Drag Coefficient

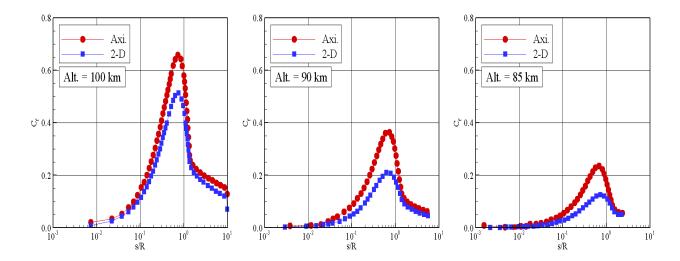The total drag coefficient C_d is defined as being,

Figure 9. Distribution of skin friction coefficient C_f along the capsule surface for altitudes of (a) 100 km, (b) 90 km, and (c) 85 km.
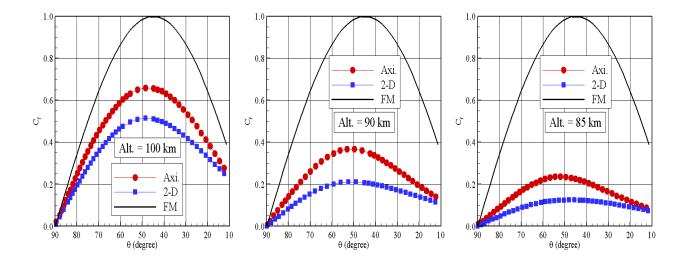
Figure 10. Distribution of skin friction coefficient C_f along the capsule surface as a function of the body slope angle θ for altitudes of (a) 100 km, (b) 90 km, and (c) 85 km.

$$C_d = \frac{F_D}{\frac{1}{2}\rho_\infty V_\infty^2 A} \tag{7}$$

where F_D is the resultant force acting on the capsule surface and A is a reference area.

The drag force F_D is obtained by the integration of the pressure p_w and shear stress τ_w distributions along the capsule surface. In the present account, the integration was considered from the stagnation point to the station that corresponds to the sphere/cone junction, for axisymmetric case, and to the cylinder/wedge, for the 2-D case. As a result, the reference area A was considered as the frontal area at this station, which is different for the two cases. In addition, no base pressure effects were taken into account on the calculations.

Changes in the total drag coefficient C_d due to variations on the altitude, or on the Knudsen number Kn_R, are displayed in Figures (11a-b) for axisymmetric and 2-D cases, respectively. In this set of diagrams, the contributions of the pressure C_{pd} and skin friction drag C_{fd} to the total drag coefficient C_d are also illustrated. According to these plots, it is noticed that, as the altitude decreases from 100 km to 85 km, the total drag coefficient C_d decreases, and the pressure drag coefficient C_{pd} plays a significant part in the total drag coefficient, a characteristic of a blunt body. It should
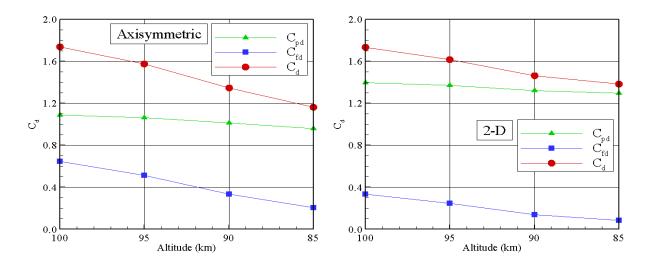

Figure 11. Pressure drag C_{pd}, skin friction drag C_{fd}, and total drag C_d as a function of the altitude for (a) axisymmetric and (b) two-dimensional cases.

be emphasized that the total drag coefficient C_d decreases as the altitude decreases because the denominator of Eq. (7) increases with an altitude reduction. On the other hand, the total drag force, F_D increases with a reduction in the altitude.

7. CONCLUDING REMARKS

Computations of a rarefied hypersonic flow over the SARA capsule have been performed by using the Direct Simulation Monte Carlo method. The calculations provided information concerning the nature of the aerodynamic surface quantities by considering planar two-dimensional and axisymmetric configurations.

Effects of rarefaction on the number flux, heat transfer, pressure, skin friction and drag coefficients were investigated for a representative altitude range, covering a hypersonic flow from the free molecular flow regime to the transitional flow regime. The altitude varied from 100 to 85 km, which correspond to Knudsen numbers Kn_R from 0.4615 to 0.0289, respectively.

The analysis showed that the stagnation region is a thermally stressed zone, as expected. The peak value for the heat flux was attained at the stagnation point. It was also found that the stagnation region is a zone of strong compression, high wall pressure. In contrast, the peak value for the shear stress took place on the spherical nose surface, more precisely between the stagnation point and the sphere/cone junction. In addition, for high altitude, the pressure coefficient agreed reasonably well with that predicted by the Newtonian theory.

8. ACKNOWLEDGMENT

9. REFERENCES

Alexander, F. J., Garcia, A. L., and Alder, B. J., 1998. "Cell Size Dependence of Transport Coefficient in Stochastic Particle Algorithms". Physics of Fluids, Vol. 10, No. 6, pp. 1540–1542.

Alexander, F. J., Garcia, A. L., and Alder, B. J., 2000. "Erratum: Cell Size Dependence of Transport Coefficient in Stochastic Particle Algorithms". Physics of Fluids, Vol. 12, No. 3, pp. 731–731.

Bird, G. A., 1981. "Monte Carlo Simulation in an Engineering Context". In Fisher, S. S., ed., Progress in Astronautics and Aeronautics: Rarefied gas Dynamics, Vol. 74, part I, AIAA New York, pp. 239–255.

Bird, G. A., 1989. "Perception of Numerical Method in Rarefied Gasdynamics". In Muntz, E. P., Weaver, D. P., and Capbell, D. H., eds., Rarefied Gas Dynamics: Theoretical and Computational Techniques, Vol. 118, Progress in Astronautics and Aeronautics, AIAA, New York, pp. 374–395.

Bird, G. A., 1994. Molecular Gas Dynamics and the Direct Simulation of Gas Flows, Oxford University Press.

Borgnakke, C. and Larsen, P. S., 1975. "Statistical Collision Model for Monte Carlo Simulation of Polyatomic Gas Mixture". Journal of Computational Physics, Vol. 18, No. 4, pp. 405–420.

Carlson, H. A., 1999. "Aerothermodynamic Analyses of Hypersonic Blunt-Body Flows". Journal of Spacecraft and Rockets, Vol. 36, No. 6, pp. 912–915.

Fay, J. A. and Riddell, F. R., 1958. "Theory of Stagnation Point Heat Transfer in Dissociated Air". Journal of Aeronautical Sciences, Vol. 25, No. 2, pp. 73–85.

Garcia, A. L., and Wagner, W., 2000. "Time Step Truncation Error in Direct Simulation Monte Carlo". Physics of Fluids, Vol. 12, No. 10, pp. 2621–2633.

Gilmore, M. R., and Crowther, R., 1995. "Direct Simulation and Test Particle Monte-Carlo, and Navier-Stokes Predictions of the Re-entry state of the FSW-1 Satellite". In Harvey, J. and Lord, G., eds., Proceedings of the 19th International Symposium on Rarefied Gas Dynamics, Oxford, University Press, Vol. 2, pp. 1387–1393.

Gnoffo, P., 1999. "Planetary-Entry Gas Dynamics". Annual Review of Fluid Mechanics, Vol. 31, pp. 459–494.

Gupta, R. N., Moss, J. N., and Price, J. M., 1996. "Assessment of Thermochemical Nonequilibrium and Slip Effects for Orbital Reentry Experiment (OREX)". In Proceedings of the 31st AIAA Thermophysics Conference, AIAA Paper 1996–1859, 17–20 Jun, New Orleans, LA.

Hadjiconstantinou, N. G., 2000. "Analysis of Discretization in the Direct Simulation Monte Carlo". Physics of Fluids, Vol. 12, No. 10, pp. 2634–2638.

Ivanov, M. S., Markelov, G. N., Gimelshein, S. F., Mishina, L. V., Krylov, A. N., and Grechko, N. V., 1998. "High-Altitude Capsule Aerodynamcis with Real Gas Effects". Journal of Spacecraft and Rockets, Vol. 35, No. 1, pp. 16–22.

Lees, L., 1956. "Laminar Hat Transfer Over Blunt-Nosed Bodies at Hypersonic Flight Speeds". Jet Propulsion, Vol. 26, No. 4, pp. 259–269.

Longo, J. M. A., 2003. "Aerothermodynamics – A Critical Review at DLR". Aerospace Science and Techonology, Vol. 7, pp. 429–438.

Machado, H., and Boas, J., 2006. "Cálculo da Pressão em Superfícies Sujeitas a Aquecimento Aerodinâmico". Proceed-

ings of the 11th Brazilian Congress of Thermal Sciences and Engineering, Curitiba, PR, Brazil.

Moss, J. N., Glass, C. E., and Greene, F. A., 2006. "Blunt Body aerodynamics for Hypersonic Low Density Flows". In Proceedings of the 25th International Symposium on Rarefied Gas Dynamics, Saint Petersburg, Russia.

Pessoa Filho, J. B., 2008. "Velocity-altitude map for SARA capsule". Private Communication.

Pimentel, C. A. R., Azevedo, J. L. F., Korzenowski, H., and Mantelli, M. B. H., 2005. "Chemical Equilibrium Inviscid Flow over SARA Re-Entry Vehicle". In Proceedings of the 43rd AIAA Aerospace Sciences Meeting and Exhibit, AIAA Paper 2005–0390, 10–13 Junuary, Reno, NV.

Roming, M., 1958. "Stagnation Point Heat Transfer for Hypersonic Flow". Jet Propulsion, Vol. 26, No. 12, pp. 1098–1101.

Sampaio, P. A. C., and Santos, W. F. N., 2009. "Aerothermodynamic Analysis of a Reentry Brazilian Satellite". In Proceedings of the 30th Iberian-Latin-American Congress on Computational Methods in Engineering, Armação de Búzios, RJ, Brazil.

Savino, R., Fumo, M. S., Paterna, D., and Serpico, M., 2005. "Aerothermodynamic Study of UHTC-Based Thermal Protection Systems". Aerospace Science and Techonology, Vol. 9, pp. 151–160.

Sharipov, F., 2003. "Hypersonic Flow of Rarefied Gas Near the Brazilian Satellite During its Reentry into Atmosphere". Brazilian Journal of Physics, Vol. 33, No. 2, pp. 398–405.

Sibulkin, M., 1952. "Heat Transfer Near the Forward Stagnation Point of a Body of Revolution". Journal of Aeronautical Sciences, Vol. 19, No. 8, pp. 570–571.

Tchuen, G., Burtschell, Y., and Zeitoun, D. E., 2005. "Numerical Prediction of Nonequilibrium Hypersonic Flow Around Brazilian Satellite SARA". Brazilian Journal of Physics, Vol. 35, No. 1, pp. 148–156.

Toro, P. G. P., Minucci, M. A. S., Ramos, A. G., Chanes Jr., J. B., Pereira, A. L., Korzenowski, H., Nagamatsu, H. T., and Myrabo, L. N., 2001. "Experimental Investigation of blunt Body at Mach 8". In Proceedings of the 39th AIAA Aerospace Sciences Meeting and Exhibit, AIAA Paper 2001–0644, 8–11 Junuary, Reno, NV.

Vashchenkov, P. V., and Ivanov, M. S., 2002. "Numerical Analysis of High-Altitude Aerothermodynamics of Expert Reentry Vehicle". In Proceedings of the International Conference on the Methods of Aerophysical Research, Russia.

Weiland, C., Longo, J., Gülhan, A., and Decker, K., 2004. "Aerothermodynamics for Reusable Lanch Systems". Aerospace Science and Techonology, Vol. 8, pp. 101–110.

Wilmoth, R. G., Mitcheltree, R. A., and Moss, J. N., 1997. "Low-Density Aerodynamics of the Stardust Sample Return Capsule". In Proceedings of the 32nd AIAA Thermophysics Conference, AIAA Paper 1997–2510, 23–25 Jun, Atlanta, GA.

Wood, W. A., Gnoffo, P. A., and Rault, D. F. G., 1996. "Aerodynamic Analysis of Commercial Experiment Transporter Re-Entry Capsule". Journal of Spacecraft and Rockets, Vol. 33, No. 5, pp. 643–646.

Zuppardi, G. and Verede, G., 1998. "Improved Fay-Riddell Procedure to Compute the Stagnation Point Heat Flux". Journal of Spacecraft and Rockets, Vol. 35, No. 3, pp. 403–405.

10. RESPONSIBILITY NOTICE

The authors are the only responsible for the printed material included in this paper.